Improved Impact Toughness of 13Cr Martensitic Stainless Steel Hardened by Laser

L.W. Tsay, Y.M. Chang, S. Torng, and H.C. Wu

(Submitted 14 November 2000; in revised form 16 October 2001)

The impact toughness of AISI 403 martensitic stainless steel plate and laser-hardened specimens tempered at various temperatures were examined. Phosphorus was the primary residual impurity responsible for tempered embrittlement of this alloy. The experimental result also indicated that AISI 403 stainless steel was very sensitive to reverse-temper embrittlement. The improved impact toughness of the laser-hardened specimen was attributed to the refined microstructure in the laser-hardened zone.

Keywords impact toughness, intergranular fracture, laser-hardening, temper embrittlement

1. Introduction

The 13 wt.% Cr martensitic stainless steels (e.g., AISI 403, 410, 420, and 422) are well-known materials for application in steam turbine blades, marine turbine blades, or compressor blades. They are generally heat-treated to provide moderate corrosion resistance and good mechanical properties. For plain 13 Cr steel, a slightly secondary hardening effect is observed in the vicinity of 500 °C after tempering,[1] which can be attributed to the precipitation of $Cr_{23}C_6$ carbides heterogeneously distributed in the martensite matrix.[2] If AISI 403 martensitic stainless steel is tempered in the temperature range between 500-680 °C, severe sensitization owing to the precipitation of large $Cr_{23}C_6$ precipitates leads to the loss of corrosion resistance of the steel.[1] In addition, hardened stainless steels that are tempered in the temperature range between 450-575 °C, or that experience slow cooling through this temperature range, will result in the progressive loss of impact toughness of the alloy, which is the so-called temper embrittlement.[3-5]

Prabhu et al.[4] report that the embrittlement of 13 wt.% Cr steels begins at 450 °C, reaches a maximum at 550 °C, and decreases with further increases in tempering temperatures. This character is believed to be caused by the segregation of impurities such as P and Sb along the prior austenite grain boundaries.[3-6] The degradation of toughness results from the weakened grain boundaries, so that its fracture mode is associated with the intergranular fracture. It is reported that P can cosegregate with Cr to the grain boundaries.[6] Moreover, it also has been reported[7] that the existence of Mn and Si promotes P segregation to the grain boundaries. Mo can act as an effective scavenger for P and other embrittling impurities, but the scavenging effect is lost when Mo is taking part in precipitating as a carbide, as a result of continuous tempering at high temperatures or service at elevated temperatures.[8] In addition, it has been pointed out that the detrimental effect of P can be greatly reduced by refining the prior austenite grain size.[9]

Laser-surface-hardening is used alternatively to modify the surface properties of many alloys.[10,11] The combination of high power density and short interaction time over the treated area for this specific process results in the low distortion of the work piece.[12,13] Selective surface treatment together with a rapid thermal cycle of laser material-processing is found to improve the hardness, wear, and fatigue properties of the work pieces.[14-18] In this study, the impact toughness of AISI 403 martensitic stainless steel tempered at various temperatures was determined. The effect of laser surface-hardening on the modification of impact toughness of this steel also was evaluated. Fractographic examinations were conducted on the fractured specimens in order to correlate the change in fracture modes with the impact toughness of the specimens.

L.W. Tsay and **Y.M. Chang,** Institute of Material Engineering, National Taiwan Ocean University, Keelung 202, Taiwan, Republic of China; **S. Torng,** Materials and Electro-optics Research Division, Chung-Shan Institute of Science & Technology, Lung Tan 325, Taiwan, Republic of China; and **H.C. Wu,** Power Research Institute, Taipei 238, Taiwan, Republic of China. Contact e-mail: b0186@mail.ntou.edu.tw.

2. Experimental Procedures

The chemical composition of the AISI 403 stainless steel used for the test was 12.2 wt.% Cr, 0.12 wt.% C, 0.38 wt.% Si, 0.48 wt.% Mn, 0.018 wt.% P, 0.01 wt.% S, 0.12 wt.% Ni, 0.032 wt.% Mo, and Fe balance. The 7.0 mm thick steel plates were austenized at 1020 °C for 40 min and subsequently were quenched by argon to room temperature. Tempering treatments were performed at 482 °C (900 °F), 538 °C (1000 °F), 593 °C (1100 °F), or 648 °C (1200 °F), respectively, for 2 h. A Rofin-Sinar 5 kW CO_2 laser with a computer-controlled working table was used for the laser surface treatment. Before laser treatments, the steel plates subjected to 648 °C tempering treatment were sprayed with a black carbon paint in order to enhance the surface absorption of the laser energy of the specimen. Surface melting was avoided by using a rectangular beam featuring a uniform distribution of laser energy over the area of 6 × 25 mm. Therefore, a more homogeneously hardened zone could be provided after laser treatment.

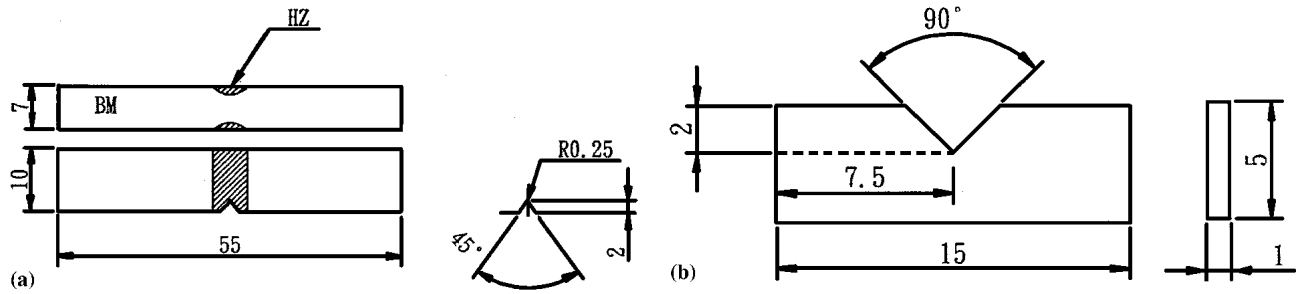

Fig. 1 A schematic diagram shows the dimensions of (**a**) a Charpy impact specimen and (**b**) an impact fracture specimen for Auger spectroscopy analysis. All dimensions are in millimeters.

In order to avoid the cold cracking of the hardened zone, all specimens were preheated at 200 °C before being irradiated by the laser beam. After the surface temperature of the hardened zone decreased to 200 °C, the laser surface treatment was performed again at the symmetrical location on the other sides of the specimen, and then the laser-hardened specimen was heated in a prolonged manner at 200 °C for 1 h. Such a specimen was designated as the L-hardened specimen. To evaluate the effect of tempering treatments on both the change of surface hardness and the impact energy of the laser-hardened specimen, a series of tempering treatments was performed. For the L-hardened specimen subjected to tempering treatment, a digital number behind the L symbol stands for the subsequent tempering temperature. For instance, L-482 represents the L-hardened specimen subjected to a 482 °C (900 °F) tempering treatment for 2 h. Furthermore, the laser-hardened specimens after tempering at various temperatures were sectioned transverse to the laser scan direction to facilitate metallographic examinations and microhardness measurements.

Figure 1 shows the dimensions of the Charpy impact specimen and impact fracture specimen, respectively, for the Auger spectroscopy analysis used in this work. The notch tip was located at the centerline of the hardened zone. The impact-fractured appearance of laser-hardened specimen at room temperature mainly consisted of the hardened zones on the outer surfaces and an interior base metal that had been tempered previously at 648 °C for 2 h. A scanning Auger microscope (model 660, PerkinElmer, Eden Prairie, MN) was used to detect the segregation of alloy elements. An in situ impact fracture was made with the pressure reduced to 2×10^{-10} torr. The segregation of impurities in the test sample was determined from the peak height ratio of P and Fe. Fractographic observations of the impact-fractured specimens were made by a Hitachi 4100 (Tokyo, Japan) scanning electron microscope (SEM).

3. Results and Discussion

Figure 2 displays the microhardness depth profiles for laser-hardened specimens with various laser scan rates. The laser power was 1200 W, and the scan rates were set at 600, 800, 1000, and 1200 mm/min, respectively. In general, the hardened zone was semi-elliptical in cross-section because the surface heat was dissipated more rapidly via conduction at the boundary of the hardened zone (not shown here). The microhardness

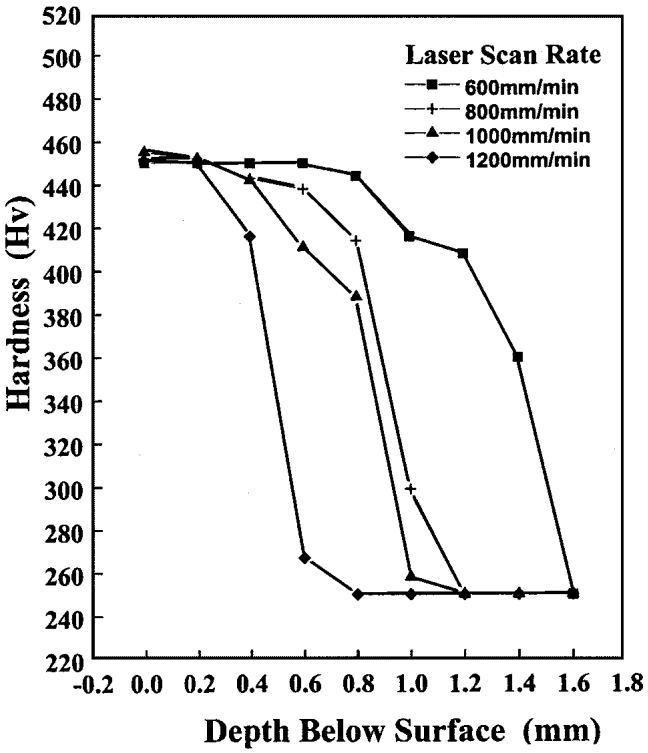

Fig. 2 The microhardness profiles of the laser-hardened specimens with different scan rates

was measured at the centerline of the hardened zone from the hardened surface into the interior base metal. This revealed that hardness decreased with increasing depth below the surface. The result also indicated that the hardened depth decreased with an increasing laser scan rate. Also, the as-hardened surface hardness in the hardened zone scanning at different rates could exceed 440 vickers hardness (HV).

Hardness vs the tempering temperature profiles for the steel plate and laser-hardened specimen are shown in Fig. 3. Figure 3(a) displays the Rockwell hardness of the steel plate after austenizing, quenching, and tempering treatments at various temperatures. The as-quenched steel plate primarily consisted of untempered martensite with a Rockwell hardness of HRC 42.8 (Fig. 3a). After the specimen was tempered at 482 °C (900 °F) for 2 h, the carbide precipitation caused a slightly secondary hardening effect with a hardness of HRC 43.1. It was noted

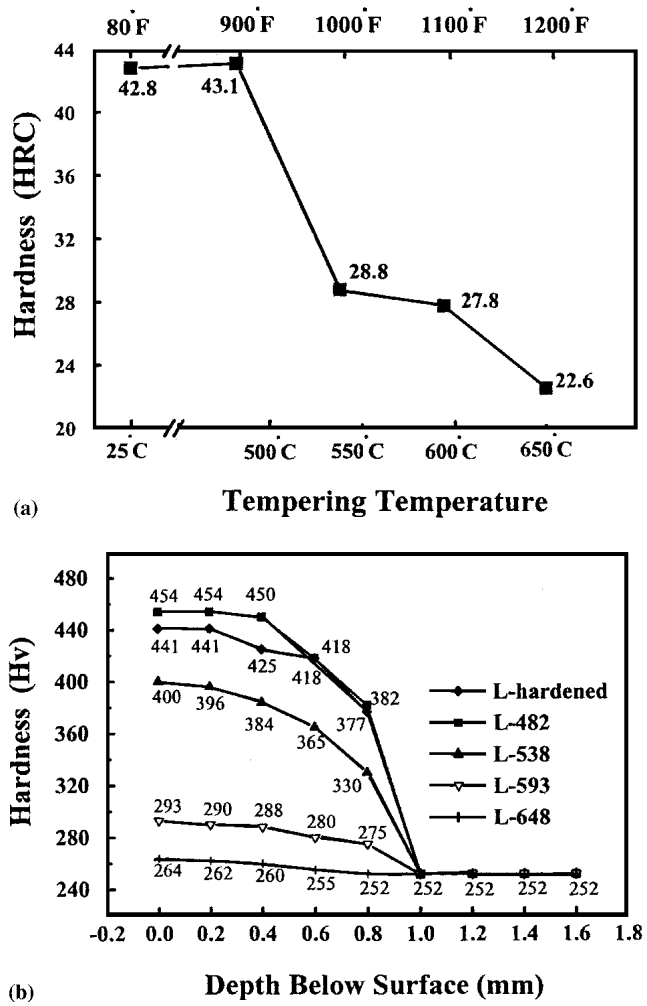

Fig. 3 The effect of tempering temperature on hardness: (**a**) the Rockwell hardness of the quenched steel plate tempered at various temperatures; and (**b**) the microhardness profiles of the laser-hardened specimens with various tempering conditions

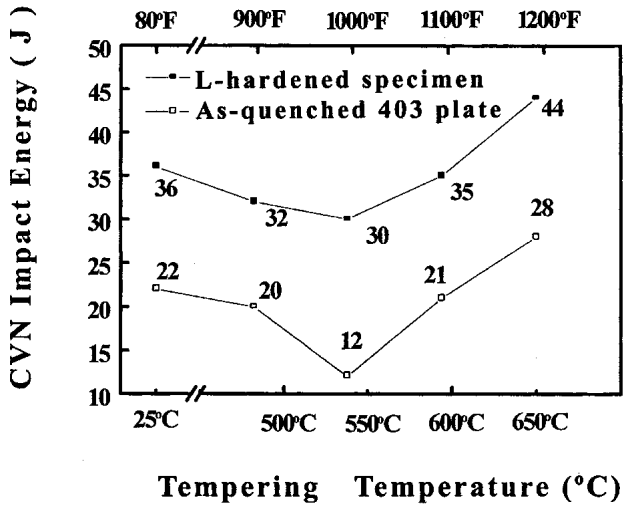

Fig. 4 Impact energy of the quenched steel plate and the laser-hardened specimens tempered at various temperatures

that the decline of hardness for AISI 403 stainless steel subjected to a 538 °C (1000 °F) tempering treatment was quite obvious, in comparison with a hardness between the steel plates tempered at 482 °C and 538 °C. A further decrease in hardness was found for these specimens that were tempered above 593 °C (1100 °F).

The curves for microhardness versus depth for laser-hardened specimens tempered at various temperatures are displayed in Fig. 3(b). The specimens had been treated previously at a laser scan rate of 1000 mm/min. Increasing the distance below the hardened surface to a depth of about 1 mm into the specimen interior, the hardness declined to the level of base metal hardness for variously tempered specimens. The surface hardness of the hardened zone in the as-hardened condition was about 460 HV. For the laser-hardened specimen after tempering at 482 °C (L-482 specimen), a secondary hardening effect could also result in a slight increase in surface hardness, as shown in Fig. 3(b). It displayed the same tendency for a change in hardness as did the steel plate. A progressive decrease in the surface hardness was found for the laser-hardened specimen tempered at higher temperatures (e.g., L-593 and L-648 specimens). The results also revealed that the hardness of the hardened zone was the same as that of the base metal in the L-648 specimen.

To compare the difference in impact energy between the steel plate and the laser-hardened specimen tempered at the same temperature, the profiles of Charpy impact energy vs tempering temperature for two types of specimens are shown in Fig. 4. The laser-hardened specimen was processed at a laser power of 1200 W and a laser scan rate of 1000 mm/min. It was noted that the structure of the laser-hardened specimen is quite similar to that of a composite material. It consisted of hardened zones on the specimen's outer surfaces and a soft interior base metal. As the crack propagated along the laser track, the measured impact energy actually represented the overall effects contributed by both the hardened zones and the interior base metal. As shown in Fig. 3(b), the additional tempering treatment below 648 °C had little influence on the decrease in base metal hardness. Regardless of the tempering temperatures, the laser-hardened specimens always had a higher impact energy than the steel plate tempered at the equivalent temperature. In addition, the impact toughness trough was found in both the steel plate and the laser-hardened specimens that had been tempered at 538 °C.

If the work piece was composed of the microstructure that previously had been tempered above 648 °C (1200 °F), reverse-temper embrittlement might occur after a long duration of service at 540 °C. In order to further confirm this evidence, a steel plate tempered at 648 °C was selected to be retempered at 538 °C, again for 2 h. Its impact energy dropped from 28 J-14 J. Thus, it clearly indicated that the AISI 403 stainless steel was very sensitive to reverse-temper embrittlement. As shown in Fig. 4, the decrease in impact toughness of the L-538 specimen could be partially attributed to the reverse-temper embrittlement of the interior base metal.

It is worth mentioning that the laser-hardened specimens tempered below 482 °C had a higher degree of hardness in the hardened zone than did the base metal. Hence, the improve-

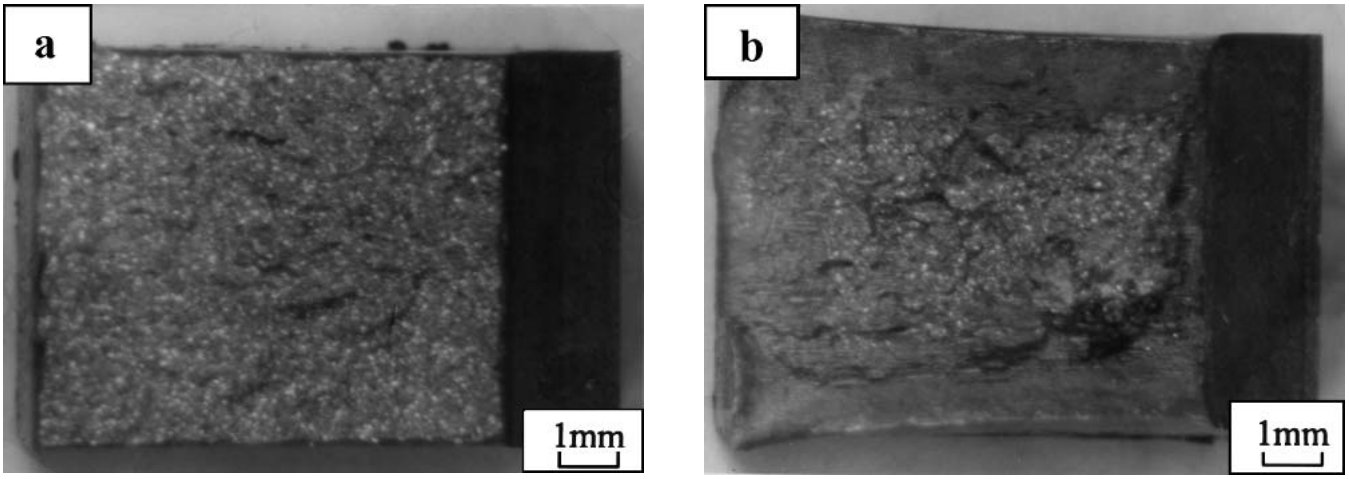

Fig. 5 Macroscopic photographs show the impact-fractured appearance of the 538 °C tempered (**a**) steel plate and (**b**) laser-hardened specimens.

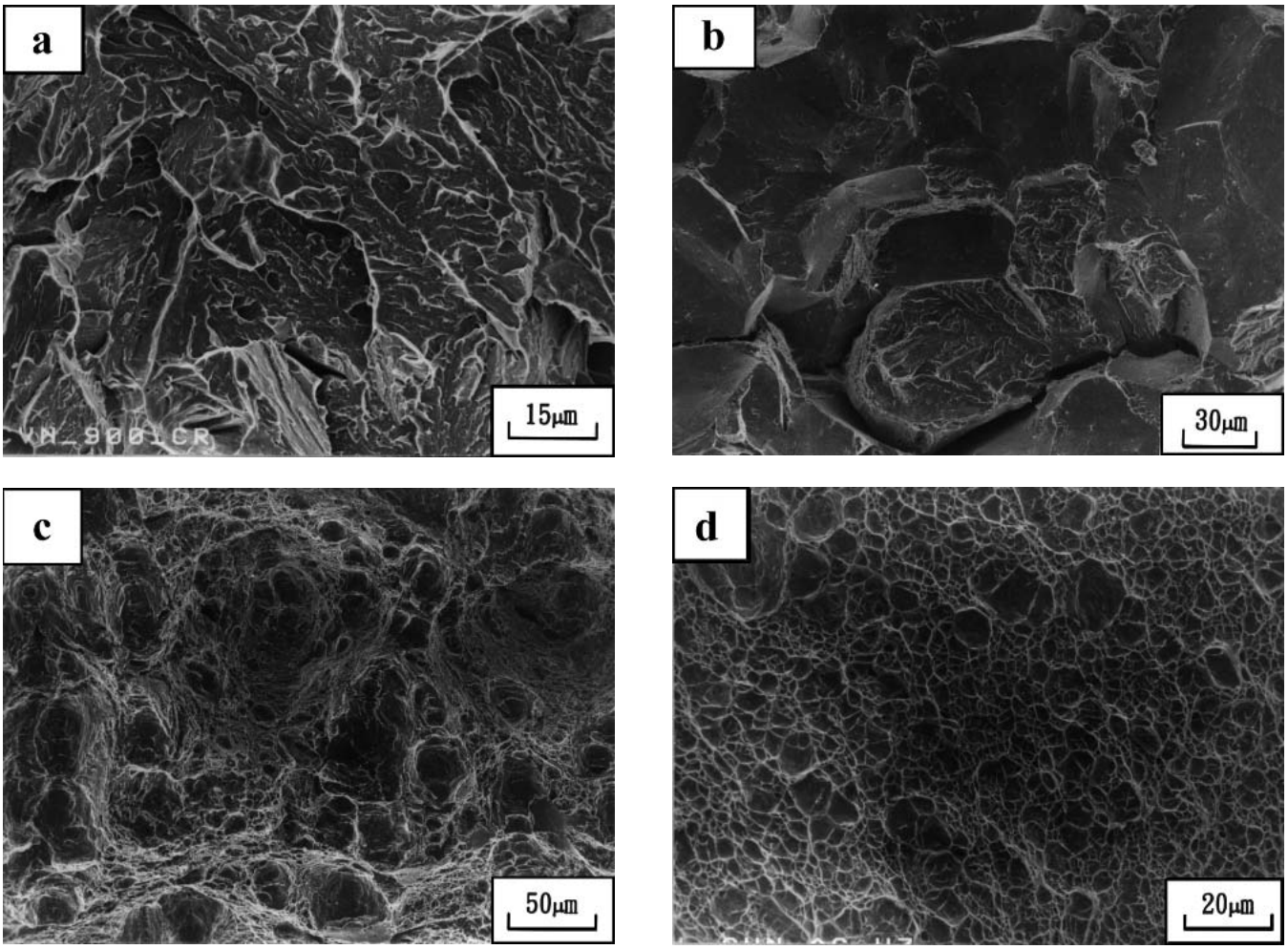

Fig. 6 SEM fractographs of impact-fractured specimens showing (**a**) a quasi-cleavage fracture of the steel plate tempered at 482 °C for 2 h, (**b**) an intergranular fracture together with few quasi-cleavages for the steel plate tempered at 538 °C for 2 h, (**c**) a ductile dimple fracture of the steel plate tempered at 648 °C for 2 h, and (**d**) a ductile dimple fracture of the laser-hardened zone tempered at 538 °C for 2 h

ment in wear resistance of such specimens would be anticipated. Furthermore, the high impact toughness of such specimens also could resist unstable crack growth more effectively than the tempered steel plate. Hence, the application of laser surface treatment on AISI 403 stainless steel to modify the surface properties should be taken into consideration.

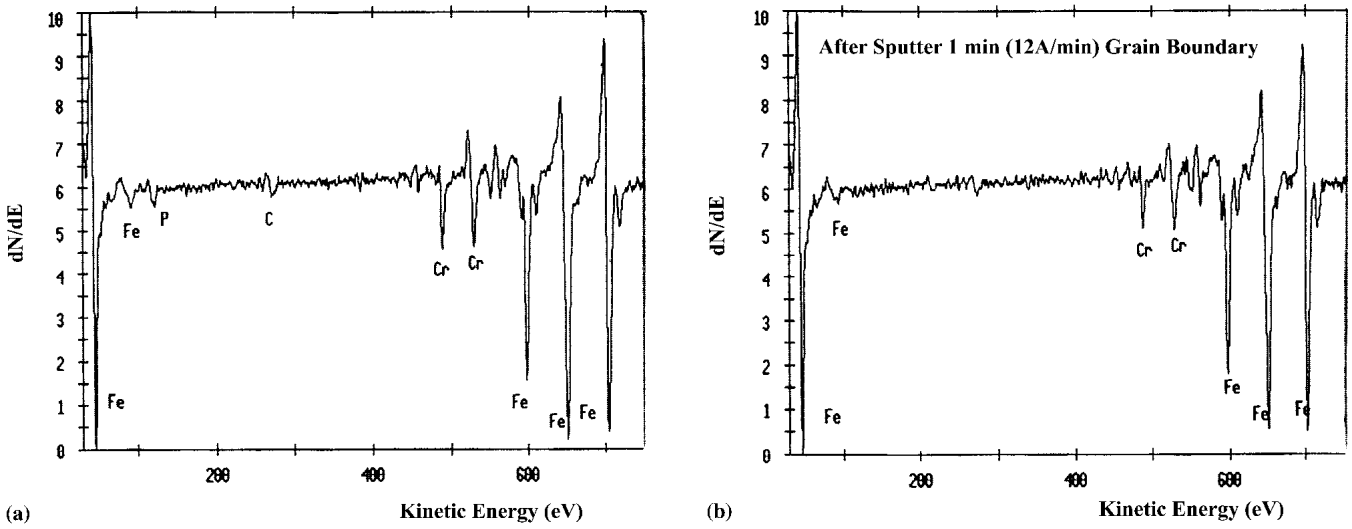

Fig. 7 Auger spectrum obtained from the fracture surface (**a**) as the fractured grain surface and (**b**) after argon sputtering

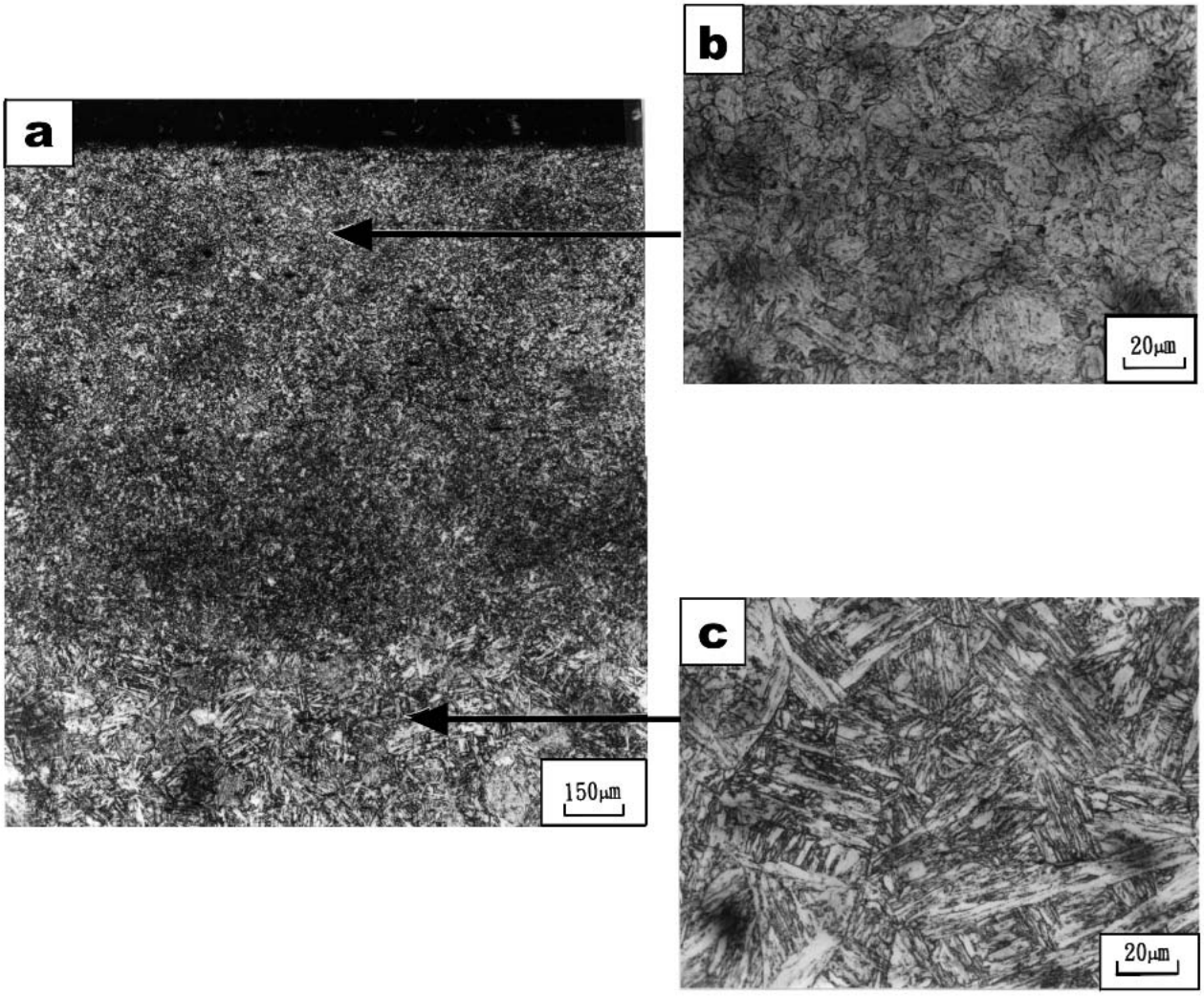

Fig. 8 Metallographs of various regions in the laser-hardened specimen tempered at 538 °C: (**a**) optical micrograph showing the microstructure of the near-surface region; and the microstructure of the (**b**) laser-hardened zone and (**c**) the base metal

As mentioned previously, both the hardened zone and the base metal had the same hardness in the L-648 specimen. It was noted that the impact toughness of the L-648 specimen was obviously higher than that of the steel plate tempered at the same temperature. Moreover, it was found that the impact energy of the laser-hardened specimen processed at a lower laser scan rate could be higher than 50 J after a 648 °C tempering treatment (not shown in this article).

Fractographs of impact-fractured specimens are shown in Fig. 5. The steel plate that had undergone temper embrittlement exhibited a rather flat fracture surface (Fig. 5a), which demonstrated the characteristics of low fracture toughness. Meanwhile, the impact fracture of the laser-hardened specimen tempered at 538 °C still consisted of shear lips on the outer surfaces, as shown in Fig. 5(b). It indicated that additional plastic deformation energy was required to extend the crack growth. Hence, it was reasonable that the laser-hardened specimen had higher impact toughness than did the steel plate. It was noted that the interior base metal of the impact-fractured L-538 specimen showed a flat fracture feature, which could be attributed to the effect of reverse-temper embrittlement therein.

SEM fractographs of impact-fractured specimens are shown in Fig. 6. A quasi-cleavage fracture was found in the as-quenched and 482 °C tempered steel plates (Fig. 6a). Fractures mainly along prior austenite grain boundaries together with a less extensive quasi-cleavage fracture indicated the detrimental effect of temper embrittlement on the 538 °C tempered steel plate (Fig. 6b). Furthermore, the fraction of intergranular fracture decreased with increasing tempering temperatures above 538 °C. The fracture appearance of the specimen tempered above 648 °C revealed a ductile dimple fracture (Fig. 6c). In contrast to crack growth along the grain boundaries for the steel plate that had experienced a loss of impact toughness, the laser-hardened zones were much more resistant to temper embrittlement, regardless of the tempering conditions. The laser hardened zone exhibited a ductile dimple fracture, as shown in Fig. 6(d).

An Auger spectrum from a freshly fractured specimen before and after argon ion sputtering is shown in Fig. 7. The Auger spectrum obtained from an intergranular fractured surface exhibited a considerable amount of P and C segregation for the 538 °C tempered steel plate (Fig. 7a). After sputtering, the grain boundary segregation of P and C diminished, as displayed in Fig. 7(b). Thus, P was the main residual impurity responsible for the embrittlement of this alloy. Metallographs of various regions for the laser-hardened specimens tempered at 538 °C are shown in Fig. 8. It was found that the microstructure of the hardened zone was much finer than that of the base metal (Fig. 8a). The microstructure in the hardened zone was too fine to be resolved by the optical microscope (Fig. 8b). In the future, further work remains to be done to identify the microstructure by transmission electron microscope (TEM). However, relatively coarse grain size was found in the base metal when comparing Fig. 8(b) and (c). It was deduced that the embrittling species distributed more uniformly in the refined microstructure, and their concentration can be greatly reduced along the grain boundaries owing to the increased boundary area. Consequently, the improved impact toughness of the laser-hardened specimen was primarily attributed to the refined microstructures in the hardened zone.

4. Conclusions

- A slight secondary hardening occurred for both the as-quenched steel plate and the laser-hardened specimen tempered at 482 °C for 2 h. A progressive decrease in surface hardness was found for the laser-hardened specimens tempered at a higher temperature. After tempering at 648 °C for 2 h, the hardened zone had the same hardness as the base metal.
- The impact toughness trough occurred for both the steel plate and the laser-hardened specimens tempered at 538 °C. Regardless of the tempering conditions, the laser-hardened specimen had a higher impact energy than did the tempered steel plate. The fracture appearance of the steel plate that had undergone temper embrittlement revealed an intergranular fracture of the specimen. The laser-hardened zone was more resistant to temper embrittlement and exhibited a ductile dimple fracture despite the tempering conditions.
- The improved toughness of the laser-hardened specimen was attributed to the refined microstructures with lower P concentration along the prior austenite grain boundaries in the laser-hardened zone.

Acknowledgments

The authors gratefully acknowledge the financial support of the Republic of China National Science Council (contract No. 89-TPC-7-019-001). The authors are indebted to Mr. Yiau-Fu Wang for his assistance in the operation of Auger microscope.

References

1. L.C. Lim, M.O. Lai, J. Ma, D.O. Northwood, and B. Miao: *Mater. Sci. Eng.*, 1993, *A171*, p. 13-19.
2. B. Miao, D.O. Northwood, L.C. Lim, and M.O. Lai: *Mater. Sci. Eng.*, 1993, *A171*, p. 21-33.
3. Ph. Lemblé A. Pineau, J.L. Castagne, Ph. Dumoulin, and M. Guttmann: *Metal Sci.*, 1979, *13*, p. 496-502.
4. G.V. Prabhu Gaunkar, A.M. Huntz, and P. Lacombe: *Metal Sci.*, 1980, *14*, p. 241-52.
5. S.K. Bhambri: *J. Mater. Sci.*, 1986, *21*, p. 1741-46.
6. R. Guillou, M. Guttmann, and Ph. Dumoulin: *Metal Sci.*, 1981, *15*, p. 63-72.
7. J.C. Murza and C.J. McMahon, Jr.: *J. Eng. Mater. Technol.*, 1980, *102*, p. 369-75.
8. Z. QU and C.J. McMahon, Jr.: *Metal Trans.*, 1983, *14A*, p. 1101-108.
9. J.H. Bulloch and J.J. Hickey: *Theor. App. Fract. Mech.*, 1994, *20*, p. 141-47.
10. M.F. Ashby and K.E. Easterling: *Acta Metall.*, 1984, *32*, p. 1935-48.
11. R.K. Shiue and C. Chen: *Metal Trans.*, 1992, *23A*, p. 163-69.
12. J. Mazumder: *J. Metals*, 1983, *35*, p. 18-26.
13. A.K. Mathur and P.A. Molian: *J. Eng. Mater. Technol.*, 1985, *107*, p. 200-207.
14. L. Ahman: *Metal Trans.*, 1984, *15A*, p. 1829-35.
15. H. De Beurs and J. Th. M. De Hosson: *Scripta Metall.*, 1981, *21*, p. 627-32.
16. H.B. Singh, S.M. Copley, and M. Bass: *Metal Trans.*, 1981, *12A*, p. 138-40.
17. S. Kocanda and D. Natkaniec: *Fatigue Fract. Eng. Mat. Struct.*, 1992, *15*, p. 1237-49.
18. L.W. Tsay and Z.W. Lin: *Fatigue Fract. Eng. Mat. Struct.*, 1998, *21*, p. 1549-58.